Environment International 170 (2022) 107575

Contents lists available at ScienceDirect

Environment International

journal homepage: www.elsevier.com/locate/envint

Full length article

Hyperlocal variation of nitrogen dioxide, black carbon, and ultrafine particles measured with Google Street View cars in Amsterdam and Copenhagen

Jules Kerckhoffs [a,1,*], Jibran Khan [b,c,1], Gerard Hoek [a], Zhendong Yuan [a], Ole Hertel [d], Matthias Ketzel [b,e], Steen Solvang Jensen [b], Fares Al Hasan [a], Kees Meliefste [a], Roel Vermeulen [a,f]

[a] Institute for Risk Assessment Sciences, Utrecht University, Utrecht, the Netherlands
[b] Department of Environmental Science, Aarhus University, Roskilde, Denmark
[c] Danish Big Data Centre for Environment and Health (BERTHA), Aarhus University, Roskilde, Denmark
[d] Department of Ecoscience, Aarhus University, Roskilde, Denmark
[e] Global Centre for Clean Air Research (GCARE), University of Surrey, Guildford, United Kingdom
[f] Julius Centre for Health Sciences and Primary Care, University Medical Centre, University of Utrecht, the Netherlands

ARTICLE INFO

Handling Editor: Xavier Querol

Keywords:
Hyperlocal air quality
Google Street View
Mixed-effect model
Exposure
Ultrafine particles

ABSTRACT

Hyperlocal air quality maps are becoming increasingly common, as they provide useful insights into the spatial variation and sources of air pollutants. In this study, we produced several high-resolution concentration maps to assess the spatial differences of three traffic-related pollutants, Nitrogen dioxide (NO_2), Black Carbon (BC) and Ultrafine Particles (UFP), in Amsterdam, the Netherlands, and Copenhagen, Denmark. All maps were based on a mixed-effect model approach by using state-of-the-art mobile measurements conducted by Google Street View (GSV) cars, during October 2018 – March 2020, and Land-use Regression (LUR) models based on several land-use and traffic predictor variables.

We then explored the concentration ratio between the different normalised pollutants to understand possible contributing sources to the observed hyperlocal variations. The maps developed in this work reflect, (i) expected elevated pollution concentrations along busy roads, and (ii) similar concentration patterns on specific road types, e.g., motorways, for both cities. In the ratio maps, we observed a clear pattern of elevated concentrations of UFP near the airport in both cities, compared to BC and NO_2.

This is the first study to produce hyperlocal maps for BC and UFP using high-quality mobile measurements. These maps are important for policymakers and health-effect studies, trying to disentangle individual effects of key air pollutants of interest (e.g., UFP).

1. Introduction

Traffic-related air pollution is highly variable in space and time, making its spatial variation difficult to assess with routine monitoring stations. Such monitoring stations are best suited for capturing the temporal variation of air pollution, including long-term trends but lack information on the street-by-street (hyperlocal) spatial differences in pollution (Li et al. 2019). An efficient way of mapping the small-scale variation of air pollution (compared to routine monitoring) is mobile monitoring (Apte et al. 2017; Hankey and Marshall 2015; Hasenfratz et al. 2015; Hatzopoulou et al. 2017; Kerckhoffs et al. 2021; Larson, Henderson, and Brauer 2009; Messier et al. 2018; Sabaliauskas et al. 2015; Shairsingh et al. 2019). This is because mobile monitoring (sampling without stopping), with a limited number of monitoring devices, enables efficient sampling in more spatially diverse environments in relatively little time.

In recent years, mobile air pollution monitoring, has taken a step forward by implementing fast-response laboratory-grade instruments in

Abbreviations: AMS, Amsterdam; BC, Black Carbon; CPH, Copenhagen; GIS, Geographic Information Systems; GPS, Global Positioning System; GSV, Google Street View; LUR, Land-use Regression; NO_2, Nitrogen dioxide; UFP, Ultrafine particles.

* Corresponding author.
E-mail address: j.kerckhoffs@uu.nl (J. Kerckhoffs).

[1] Shared first authors.

https://doi.org/10.1016/j.envint.2022.107575
Received 18 March 2022; Received in revised form 3 October 2022; Accepted 7 October 2022
Available online 8 October 2022

mobile platforms. Apte et al. (2017) and Messier et al. (2018) demonstrated that such an approach could reveal urban pollution gradients and efficiently map long-term average air quality at a high spatial resolution based on measurements alone. However, mobile monitoring is labour intensive, as it requires all streets to be driven multiple times. This is done to derive a reliable estimate of the long-term mean concentration of a street segment. However, measuring each street segment multiple times in a large region might not be feasible and scalable to large areas.

On the other hand, most Land-use Regression (LUR) and dispersion models tend to smooth concentration levels over similar locations or a wider terrain (Hoek 2017). Either by using prediction variables with a coarse spatial resolution or averaging concentrations over locations with similar spatial characteristics. This way some of the hyperlocal variation of air pollution in cities is lost.

We recently described a mixed-effect modelling framework, combining the advantages of "data-only" mapping and LUR modelling in an associated study (Kerckhoffs et al. 2022). Specifically, it is a linear mixed-effect model, with the determinants from a linear regression model as input for the fixed-effect model and all individual street segments as the random-effect. This means that all individual measurements can influence the output of the fixed-effect model based on the measured between and within-street segment concentration variation. In Kerckhoffs et al. (2022), mobile nitrogen dioxide (NO_2) measurements were carried out using Google Street View (GSV) cars in Amsterdam and Copenhagen. The mixed-effect modelling framework has been extensively explained and validated, demonstrating the feasibility of the adopted approach to develop high-resolution NO_2 concentration maps for Amsterdam and Copenhagen with better performance than data-only and LUR-only approaches. In this paper, we extend the mixed-effect modelling approach to UFP and BC.

Kerckhoffs et al. (2022) also reported strongly correlated mixed-effect model predictions with external long-term passive NO_2 measurements. Here, it is important to note that multiple high-quality datasets exist for NO_2 for Amsterdam and Copenhagen. However, this is rarely the case for ultrafine particles (UFP) and black carbon (BC). Compared to NO_2, only limited routine monitoring is done for BC and minimal monitoring for UFP. To our knowledge, this is the first time mobile measurements of UFP are used to map pollution levels in all the streets of a domain of interest and one of the first street-by-street pollution maps for BC. On top of that, by measuring multiple pollutants at the same time, we are better able to highlight their differences in spatial variation within a city.

In this paper, we use data from two different cities and multiple pollutants and show the applicability of mobile monitoring using a mixed-effect model approach in two different urban environments and show spatial differences between NO_2, BC and UFP at the same time. Our focus is to assess differences in spatial variation and investigate the contribution of different combustion sources on air pollution levels. This can help disentangle individual effects of air pollutants in health-effects studies, as two- or multi-pollutant models have shown inconsistent results (Ohlwein et al. 2019; Tavallali et al. 2020). In addition, we analyse the robustness of NO_2, UFP and BC measurements when drive days are systematically decreased. Furthermore, we explore spatial patterns in the data, highlighting differences in model predictions using pollution concentrations ratio analyses.

2. Materials and methods

2.1. Study design

The study sites are the city of Amsterdam in the Netherlands, and three municipalities (Copenhagen, Frederiksberg and Tårnby) in the Copenhagen metropolitan area, Denmark, hereafter, referred to as Copenhagen.

Amsterdam (AMS) is the capital and the most populous city of the Netherlands (Fig. 1), having an approximate area of 219.4 km^2. The landscape surrounding the Dutch capital is mostly flat. The city centre contains a mix of commercial and residential buildings, and a dense network of major and minor roads. A few interstate highways can also be seen in Fig. 1. Amsterdam has an oceanic climate, significantly affected by its proximity to the North Sea to the west, with prevailing westerly winds. The Schiphol airport is located 10 km west of Amsterdam.

Copenhagen (CPH) is the Danish capital and the most populous city in the country (Fig. 1). The area is relatively flat and extends up to approx. 292.5 km^2. Like Amsterdam, the city centre of Copenhagen has a mix of residential and commercial buildings, major and minor roads. In addition, highways, and an airport (south of the city) can also be seen (Fig. 1). The Danish capital also has an oceanic climate. Its weather is influenced by low-pressure systems from the Atlantic's, resulting in westerly and south-westerly prevailing winds.

The ambient concentrations of NO_2, BC and UFP, were measured in the two cities during October 2018 – March 2020. The measurements were carried out by three GSV cars. In Amsterdam, two GSV cars measured concentrations from 25 May 2019 to 15 March 2020, whereas, in Copenhagen, the third GSV car measured pollution levels from 15 October 2018 to 15 March 2020. Both campaigns were stopped on 15 March 2020 due to Covid-19 lockdown restrictions.

The GSV cars were equipped with lab-grade fast-response 1 Hz NO_2 (CAPS, Aerodyne Research Inc., USA), 1 Hz BC (AE33, Magee Scientific), and 1 Hz UFP (EPC 3783, TSI) monitors measuring simultaneously. The

Fig. 1. The study sites, (A) the city of Amsterdam in the Netherlands, and (B) three municipalities of Copenhagen metropolitan area, Copenhagen, Frederiksberg, and Tårnby. The locations of airports and references monitors are also shown.

UFP monitor, EPC 3783, is a water-based Condensation Particle Counter (WCPC), and provides particle counts (a proxy for UFP) up to 10^6 particles/cm^3 (TSI 2022). The WCPC, compared to the CPC using, e.g. butanol as a working fluid, has a higher detection efficiency due to (i) no emissions, (ii) no cross-sensitivity towards measuring pollutants, and (iii) no water uptake (deposition) by alcohol working fluid, yielding more reliable measured data (Bischof et al. 2005; Liu et al. 2006; Spielman et al. 2017). A Global Positioning System (GPS) (G-Star IV, GlobalSat, Taiwan) was used to record the location of the car, which was linked to the measuring equipment via date and time. The measurements were mainly carried out between 08.00 and 22.00 h every day in the study period (excluding weekends and car malfunctioning) and in different parts of both cities. The aim was to reduce possible space and time autocorrelation. This was particularly relevant for Amsterdam, where two GSV cars were used.

Due to malfunctioning and internal calibration of the instrument, measured 1-second NO_2 values higher than 500 μg/m^3 and lower than 0 were discarded (0.9 % of measurements). For BC, we removed values higher than 30 μg/m^3 (0.1 % of the measurements), and for UFP, we removed values higher than 500,000 (0.1 % of the measurements) particles/cm^3 from the data as such values are not physically possible in the measured environments. Furthermore, we applied a moving average of 6 s for BC to filter out the noise of the instrument. For Amsterdam, the final data set contained 5.9, 5.8, and 5.0 million 1-second measurements of NO_2, BC and UFP, respectively. Similarly, for Copenhagen, there were 5.1, 5.0, and 5.5 million 1-second measurements of the three pollutants in the final data set.

2.2. Data protocols

As measurements were carried out at different times of the day and week, the measured data were temporally corrected using nearby routine monitoring stations (Hankey and Marshall 2015; Kerckhoffs et al. 2017, 2021; Montagne et al. 2015). The aim was to estimate longer-term average concentrations. Because of the limited availability of reference data for BC and UFP in Copenhagen, measurements were not temporally corrected. NO_2 data in CPH, and all three pollutants in AMS were temporally corrected. Applying the same procedure in Amsterdam as in Copenhagen (i.e., no correction) resulted in essentially similar models (Tables S7 and S8).

For the temporal correction, a difference correction method was used for Amsterdam, using background monitoring stations from the Dutch National Air Quality Monitoring Program (RIVM-LML 2020). First, an overall mean concentration of the whole measurement campaign was calculated at the reference station. Then, a moving average (4 h) was calculated at the same reference station. Finally, for each (1-Hz) measurement of the GSV cars, the 4-hour moving average was subtracted from the overall mean concentration and subsequently subtracted or added to the measured data.

For Copenhagen, the measured NO_2 data was corrected using reference values from a background air quality station, located at the rooftop of the H.C. Ørsted Institute, the University of Copenhagen (hereafter, HCØ). The HCØ station is part of the Danish Air Quality Monitoring Program (Ellermann et al. 2021). Due to the location of the HCØ station (measuring urban background NO_2 concentrations, only marginally influenced by nearby roads and rush hours), a ratio correction method was applied. The ratio method uses the same procedure as the difference method but instead the correction is calculated by dividing the 4-hour moving average by the overall mean concentration of the measurement campaign at the HCØ and multiplied with the on-road measured values (Kerckhoffs et al. 2022).

The corrected data was subsequently winsorised to the 2.5th and the 97.5th percentile. That is, measured concentration levels below the 2.5th percentile and above the 97.5th percentile were "replaced" by the respective percentile values (Kerckhoffs et al. 2022). This procedure is done to balance the unduly influence of extreme values, while allowing very high pollution values. For averaging, the data was first assigned to the nearest street and aggregated over each 50-meter (min: 30 m and max: 60 m) street segment per individual drive day. Most mobile monitoring studies use street segments with a distance between 30 and 100 m to aggregate mobile measurements, with (Hankey and Marshall (2015) finding limited differences between spatial aggregations between 50 and 200 m. The aggregation per street segment per drive day resulted in 346,848 and 223,047 mean street segment values, with an interquartile range of 3–9 s per drive-pass, for AMS and CPH respectively. Next, we calculated the mean of all the drive days per street segment, resulting in a "mean of means". Each street segment, on average, contained 7 unique drive days, both for AMS and CPH. In total, 46,664 and 32,270 street segments in the road networks of Amsterdam and Copenhagen were measured.

2.3. Model developments

For the main analyses, we developed a linear mixed-effect model, with fixed effects estimated based on determinants from a linear regression model and random intercepts for all individual street segments (random-effect model). Model development is extensively described in Kerckhoffs et al. (2022) and Supplementary Information of this article. Although Kerckhoffs et al. (2022) only describes the NO_2 model, UFP and BC models were developed in the same way.

In brief, we developed LUR models with a supervised linear stepwise approach using the corrected mean of means data and GIS predictors (i.e., data on road length and traffic intensity, population density and land use in different buffer sizes (50–5000 m). Supplementary Tables S1-S6 provide an overview of the selected GIS predictors for NO_2, BC and UFP LUR models for Amsterdam and Copenhagen. The variable selection process was conducted using a forward, stepwise regression method. This approach starts by taking an empty, intercept-only model, and then adds variables based on the goodness of fit determined via the adjusted R^2 values (Kerckhoffs et al. 2017; Montagne et al. 2015).

In the mixed-effect model development, selected variables from the LUR model were used as the fixed effects, and re-estimated based on all the data in the mixed-effect model. The correlation between repeated measurements on a single street segment was modelled using a random intercept. The mixed-effect model estimates are then computed as:

$$y_{ij} = \beta_0 + \beta_1 X_i + u_i + e_{ij}$$

where i indexes the street segments, j the repeated drive-days, and X_i is the matrix of variables selected from the LUR model. Both the random intercept u_i and residuals e_{ij} are assumed to follow a normal distribution centered at zero and with variance estimated using REML.

Best Linear Unbiased Prediction (BLUP) was used to include the estimated street segment effect into the final predictions to retain as much of the estimated "hyperlocal" variation as possible, while shrinking predictions for street segments with fewer or more variable measurements towards the fixed-effect model means. The re-estimated parameters (fixed-effect model) and random effect variance of the mixed-effect model of all pollutants in both cities can be found in the supplement (Tables S9-S14). Mixed-effect model estimates outperformed LUR and data-only mapping in predicting external long-term NO_2 concentrations in our previous paper (Kerckhoffs et al. 2022). We therefore use the mixed-effect model estimates of NO_2, BC and UFP as our main model.

2.4. Robustness of measured data

We assess the variation of the measured drive-pass means for all street segments by showing the standard error of the mean relative to the average concentration of the street segment (i.e., Relative Standard Error of the Mean) for all pollutants. This is calculated as the Standard Error of the Mean divided by the Mean of Means for every street

segment.

Since the number of drive days can influence measurements and underlying models, we investigated the influence of drive days on the robustness of average concentrations. We used street segments with at least 15 drive days for both cities (between 10 % and 15 % of all street segments, depending on pollutant and city). For street segments with more than 15 drive days, we randomly selected 15 drive days. Additionally, we used a subset of street segments in specific areas in Copenhagen, near the city centre (Vesterbro; Fig. 1) and the airport (Amager) without highways and with a representative classification of major and residential roads, also having a minimum of 15 drives per street segment.

We assumed that 15 drive days provide a robust "long-term" average concentration for subsequent analyses. Apte et al. (2017) performed a similar analysis on NO and BC concentrations in Oakland, but sampled all street segments in their domain at least 50 times. In Apte's study, the correlation between mean concentrations of random subsets based on 15 drives correlated about 0.9 with concentrations based on the full 50 drives. Next, we iteratively and randomly decreased the number of drive days within each street segment. We correlated the average measured value of the subset with the average measured value based on the full 15 drive days. This process was randomly repeated 30 times for each city, and the mean was recorded. Furthermore, we calculated the mean absolute percentage error (MAPE), to assess the average bias of a subset compared to the overall average.

2.5. Spatial patterns and hotspots

We explored the hyperlocal variation of NO_2, BC and UFP in Amsterdam and Copenhagen, and show the mixed-effect model estimates for all three pollutants in both cities. Similarities between pollutants are assessed by correlation statistics, whilst ratios between normalised pollutant concentrations were used to identify places where mixed-effect model estimates differ between pollutants. Here, the aim was to identify distinct sources of the pollutants (Keuken et al. 2012). The ratios of the normalised mixed-effect model estimates were calculated by dividing the estimated concentration by the mixed-effect model, by the difference between the minimum and the maximum mixed-effect model estimates of the respective pollutant. Differences between air pollutants were also analysed by looking at the absolute difference in mixed-effect model estimates between road types. For this, we assigned all street segments in AMS and CPH to a road classification adopted from OpenStreetMap (OpenStreetMap contributors 2021), being motorways, primary, secondary, tertiary and residential roads.

To highlight hotspots (and cold spots) in the air pollution maps, we performed hotspot analyses in both cities on the mixed-effect model estimates. This was done via the Getis-Ord Gi* statistic (Getis and Ord 1992) looking at street segments within 50 m. This means that at least one other street segment is considered and, in most cases, the two adjacent street segments. This statistic makes sure that street segments with a high concentration level are only considered a hotspot when it is surrounded by other street segments with high concentration levels. Specifically, the local sum for a street segment and its neighbours is compared proportionally to the sum of all street segments. When the local sum is very different from the expected local sum, and when that difference is too large to result from random chance, it is considered statistically significant. This approach ensures a more robust identification of hotspots at the cost of potentially missing very local sources that would only influence a single 50 m segment.

Another way of looking at modelled spatial variation is by inspecting differences between fixed-effect model estimates and the mixed-effect model estimates, i.e., the random-effects. Street segments with a large random-effect are of interest because they cannot be adequately explained by the fixed-effect part of the mixed-effect model. Such places might point to unknown sources or might indicate very specific local sources.

3. Results and discussions

3.1. Summary statistics

Table 1 shows the summary statistics of (temporally corrected) measurements in Amsterdam and Copenhagen. We also included distribution plots on the number of seconds per street segment per drive day, the number of drive days per street segment and the number of measured street segments per month, hour of the day and day of the week in the appendix (Figs. S1 and S2). Concentrations are, on average, higher in Amsterdam compared to Copenhagen for all pollutants. The median values of NO_2, UFP and BC for Amsterdam were 24 $\mu g/cm^3$, 17,300 particles/cm^3 and 1.1 $\mu g/cm^3$, respectively, whereas for Copenhagen, it was 13 $\mu g/cm^3$, 9,600 particles/cm^3 and 0.9 $\mu g/cm^3$. When the study period of Copenhagen was restricted to the same period as Amsterdam, the median values of NO_2, BC and UFP were 13 $\mu g/cm^3$, 9,700 particles/cm^3 and 0.8 $\mu g/cm^3$.

3.2. Robustness of measured data

Fig. 2 shows the standard error of the mean for all drive-pass means per street segment. Specifically, it shows the standard error of the mean within each street segment as a percentage of the average concentration of that street segment, multiplied by 100 to create percentages. UFP measurements (relative error IQR: 22–60 %) are much more variable across drive days, compared to NO_2 (11–26 %) and BC (13–30 %) measurements in Amsterdam. This is less so in Copenhagen, with less variability of UFP concentrations across drive means (17–39 %), but with more variability in BC concentrations (18–43 %). However, the larger variation in BC concentrations disappears when only street segments are considered with more than 10 drive days (Fig. S3). The interquartile range of BC concentrations with >10 drive days is 13–20 %, compared to 9–18 % and 14–26 % for NO_2 and UFP in CPH, respectively.

Variability over drive days in NO_2 concentrations is consistently low in both cities (AMS: 11–26 %, CPH: 12–26 %). Although this variability is temporal, it should be noted that NO_2 is a secondary pollutant, with relatively less local source influences, whereas UFP and BC are considered primary traffic pollutants.

Fig. 3 shows the influence of the number of drive days on the robustness of the mean of means. This analysis assumed that an average concentration based on at least 15 drive days is a robust, "long-term" average concentration. In a sensitivity analysis in Amsterdam and Copenhagen, we also show that the average concentration based on 15 drive days correlates very highly ($r > 0.9$) with those based on 30 drive days (Fig. S4), though on a smaller number of roads. A similar analysis was done by Apte et al. (Apte et al. 2017), with similar results. Nevertheless, the number of drive days needed for a robust estimate will depend on the pollutant, design, and geographical domain.

In general, we found that 1–2 fewer drive days of measuring NO_2 are needed to achieve a stable estimate, compared to UFP and BC, both in AMS and CPH (Fig. 3). When all street segments with at least 15 drive days in CPH were considered, we did not find a clear difference between pollutants regarding the correlation coefficients. The reason for the better correlation for UFP could be due to the influence of the airport on the concentration levels. Also, the LUR model for UFP in CPH performed considerably better than in AMS, indicating that it is easier to explain differences in UFP concentrations in CPH as compared to AMS. Differences between pollutants were more similar between cities when looking at the mean absolute percentage error (MAPE) of all pollutants. NO_2 has the lowest relative error, compared to UFP and BC. All three pollutants have very similar patterns in both cities, with UFP concentration slightly less robust in Amsterdam than Copenhagen. After 3 drive days, the MAPE is about 20 % for NO_2 but is more than 30 % for UFP and BC. This is because UFP and BC levels, as primary pollutants, generally vary more in space and time, whereas NO_2 is more of a secondary pollutant.

Table 1
Summary statistics of the corrected street-segment average measurements in Amsterdam and Copenhagen.

	Amsterdam (May 2019-March 2020)			Copenhagen (October 2018-March 2020)		
	NO_2 ($\mu g/m^3$)	UFP (particles/cm^3)	BC ($\mu g/m^3$)	NO_2 ($\mu g/m^3$)	UFP (particles/cm^3)	BC ($\mu g/m^3$)
5th percentile	14	2,800	0.6	7	4,000	0.3
25th percentile	19	11,400	0.8	10	6,700	0.6
Median	24	17,300	1.1	13	9,600	0.9
Mean	28	21,000	1.4	17	13,800	1.0
75th percentile	33	26,100	1.7	20	15,800	1.3
95th percentile	55	52,200	3.0	39	36,800	2.4

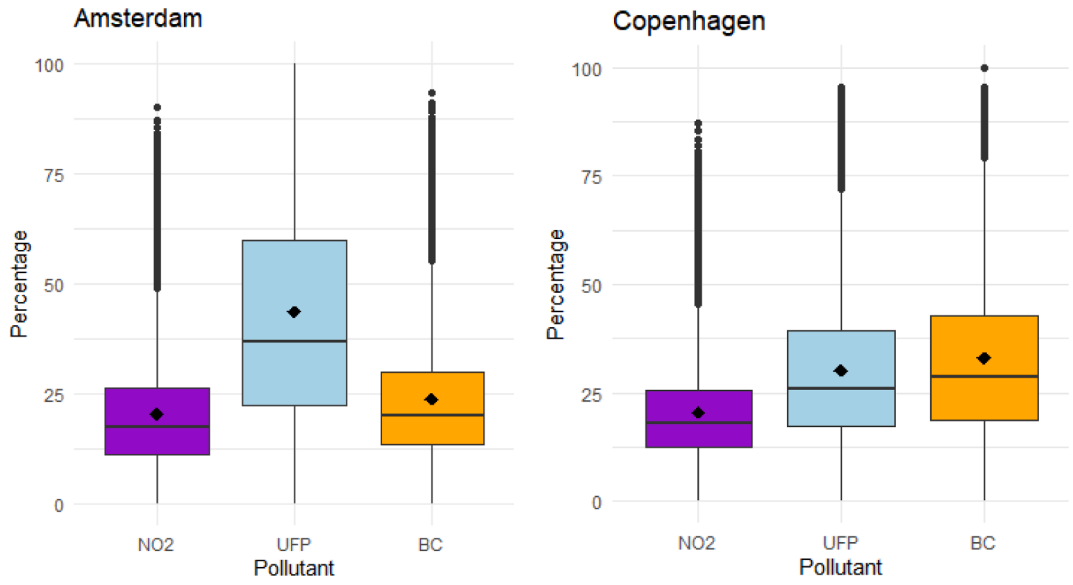

Fig. 2. Relative Standard Error of the Mean. Calculated as the Standard Error of the Mean divided by the Mean of Means for every street segment and multiplied by 100. Boxes represent the Interquartile Range (IQR); the horizontal line is the median; vertical lines extent to IQR times 1.5 (limited to data); dots are individual outliers; the black squared dot is the mean.

In addition, about 9 drive days are needed for NO_2 to achieve a relative error of less than 10 percent in both cities. While for UFP and BC, about 12 drive days are needed (Fig. 3). Fig. S5 shows a big difference between the cities in the absolute error of all pollutants. Especially with a few drive days, the absolute error in Amsterdam is about twice as high as in Copenhagen. This is mainly because concentrations for all three pollutants are higher in Amsterdam than in Copenhagen (see Table 1).

Excluding highways from the analyses slightly changes the Pearson correlation scores and MAPE scores (Fig. 3; bottom graphs). The total variation within the specific areas (e.g., Vesterbro and Amager in Copenhagen, see Fig. 1) is less than for all street segments in CPH, because highways are not included in these areas. This resulted in the correlation pattern being less spherical than for all streets in AMS and CPH. In other words, more drive days are needed in specific areas (e.g., Vesterbro) to achieve the same correlation scores, especially for UFP and BC. On the other hand, fewer drive days are needed to achieve a relative error of less than 10 percent, which is more pronounced for NO_2 compared to UFP and BC.

3.3. Spatial patterns and hotspots

All maps presented in this manuscript (overview of the cities, the mixed-effect model estimates, road network classification, ratio maps, hotspot maps and random-effect maps) for NO_2, BC and UFP, for both cities can be found as high-resolution maps in the Appendix. A zoomable, clickable format of the mixed-effect model estimates can be found on Google's Earth Insight Explorer (EIE) website (https://insights.sustainability.google/labs/airquality).

3.3.1. Correlation between pollutants

NO_2, BC and UFP are considered traffic-related air pollutants (TRAPs), correlation between mixed-effect model estimates of the three pollutants are high, r = 0.81 (0.70) for NO_2 and UFP, 0.81 (0.79) for UFP and BC and 0.93 (0.94) for BC and NO_2 in Amsterdam (and Copenhagen). High spatiotemporal correlations (r = 0.81–0.90) between NO_2 and BC were also found in a study by Gani et al. (2021), who compared hourly concentrations of UFP, NO_2 and BC in near-highway and (sub) urban settings. However, the correlation between UFP and other traffic-related air pollutants in Gani's study was lower, with r = 0.52–0.66 for UFP and NO_2 and r = 0.56–0.73 for UFP and BC. This implies that UFP both temporally and spatially differs from other traffic-related air pollutants, which can mainly be attributed to new particle formation events (Brines et al. 2015; Dall'Osto et al., 2013; Gani et al. 2021; Hofman et al. 2016). Although traffic remains the most important factor for UFP concentrations (primary pollution), several studies found that new particle formation events (secondary pollution) occur on about 13–36 % of the days(Brines et al. 2015; Hofman et al. 2016) and can contribute significantly to UFP concentrations, especially when traffic is not the only source (Dall'Osto et al., 2013).

3.3.2. Mixed-effect model estimates

Spatial patterns are highlighted in Fig. 4 with the mixed-effect model estimates of NO_2, BC and UFP in Amsterdam and Copenhagen. For all pollutants in both cities, as expected, the major roads have the highest concentrations of air pollution, which are also identified as the main

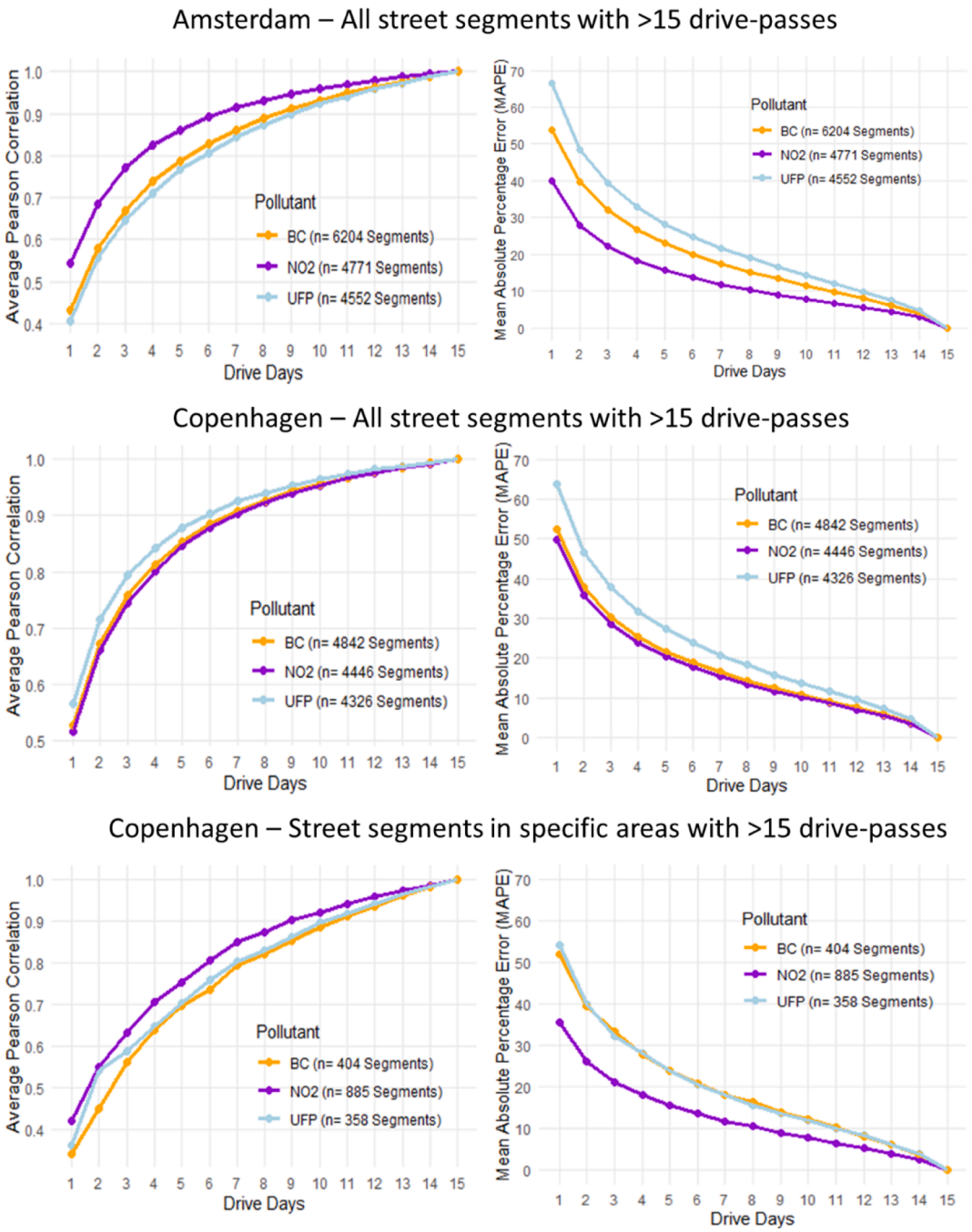

Fig. 3. Performance evaluation for subsampled measured average concentration in terms of Pearson correlation coefficients and mean absolute percentage error (MAPE) for all streets in Amsterdam with at least 15 repeats (top), all streets in Copenhagen with at least 15 repeats (middle), and streets in the specific areas (e.g., Vesterbro) in Copenhagen (Fig. 1) with at least 15 drive days (bottom).

hotspots (Fig. S6). This can also be seen by the variables in the LUR models, with all six model selecting local traffic intensity (on major roads) as the most important variable (Tables S1-S6). For UFP, this is more pronounced on the highways than the other two pollutants. UFPs quickly transform through physicochemical processes, like coagulation or condensation (Hagler et al., 2009) and can reach background levels within 300 m of a highway, with even sharper gradients for the smaller particles (Zhu et al., 2009). Since the traffic volume on highways is much more than on other roads, there are many fresh particles, resulting in the fact that only highways show up as the main hotspot for UFP, whereas this is more variable for NO_2 and BC. In addition, UFP concentrations on streets near the Copenhagen airport are clearly elevated, whereas this is not directly visible near Amsterdam airport.

3.3.3. Ratio maps

By showing the ratio between normalised concentrations of pollutants (Fig. 5), differences in spatial variation are further emphasized. The ratio maps for BC to UFP and NO_2 to UFP are very similar compared to the BC to NO_2 ratio map, both for Amsterdam and Copenhagen, meaning the difference between UFP and other pollutants is larger than for BC and NO_2. This aligns with our previous findings that UFP is different from other traffic-related air pollutants. We also observe different patterns in the BC to NO_2 maps for Amsterdam and Copenhagen. Elevated BC concentrations (compared to NO_2) can be found towards the outskirts of Amsterdam, while for Copenhagen, elevated BC levels were mainly found in Vesterbro (Fig. 1) and the southern part of the city. This can partly by explained by the fact that BC is related to diesel emission

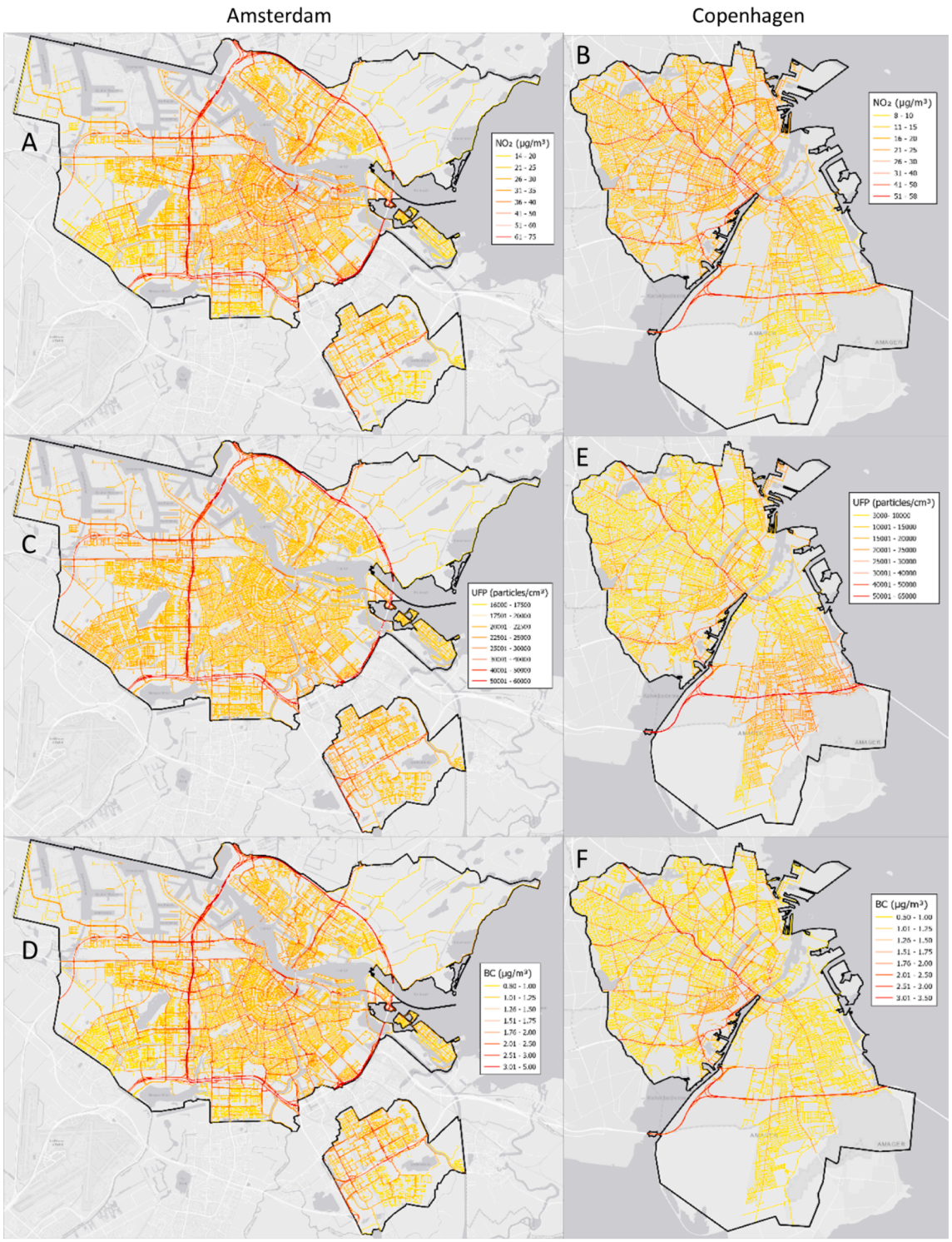

Fig. 4. Mixed-effect model predictions for (A, B) NO_2, (C, D) UFP and (E, F) BC concentrations levels in Amsterdam and Copenhagen. Scales differ between cities to show contrast.

and extensive road (and metro) constructions in the area. In other parts of the city, elevated BC concentration is also associated with wood burning, which might explain elevated concentration levels in certain neighbourhoods.

Another clear pattern in the spatial variation is the increased UFP concentrations near Amsterdam and Copenhagen airports (Fig. 5). However, as stated above, concentrations near Amsterdam airport were relatively lower than those near Copenhagen airport. Emissions from ascending and descending aircraft can significantly impact UFP concentrations up to 10 km downwind (Hudda et al. 2014). While the impact of the airport in Amsterdam on UFP concentrations is not clearly visible in Fig. 4, it can better be seen in Fig. 5. Concentrations drop for all pollutants going from urban to suburban settings, but not for UFP in the airport direction. LUR models for UFP in both cities include the airport as a predictor in the model (Table S2 and S4), similar to most UFP studies that are close to airports (Hatzopoulou et al. 2017; Jones et al. 2020; Weichenthal et al. 2015).

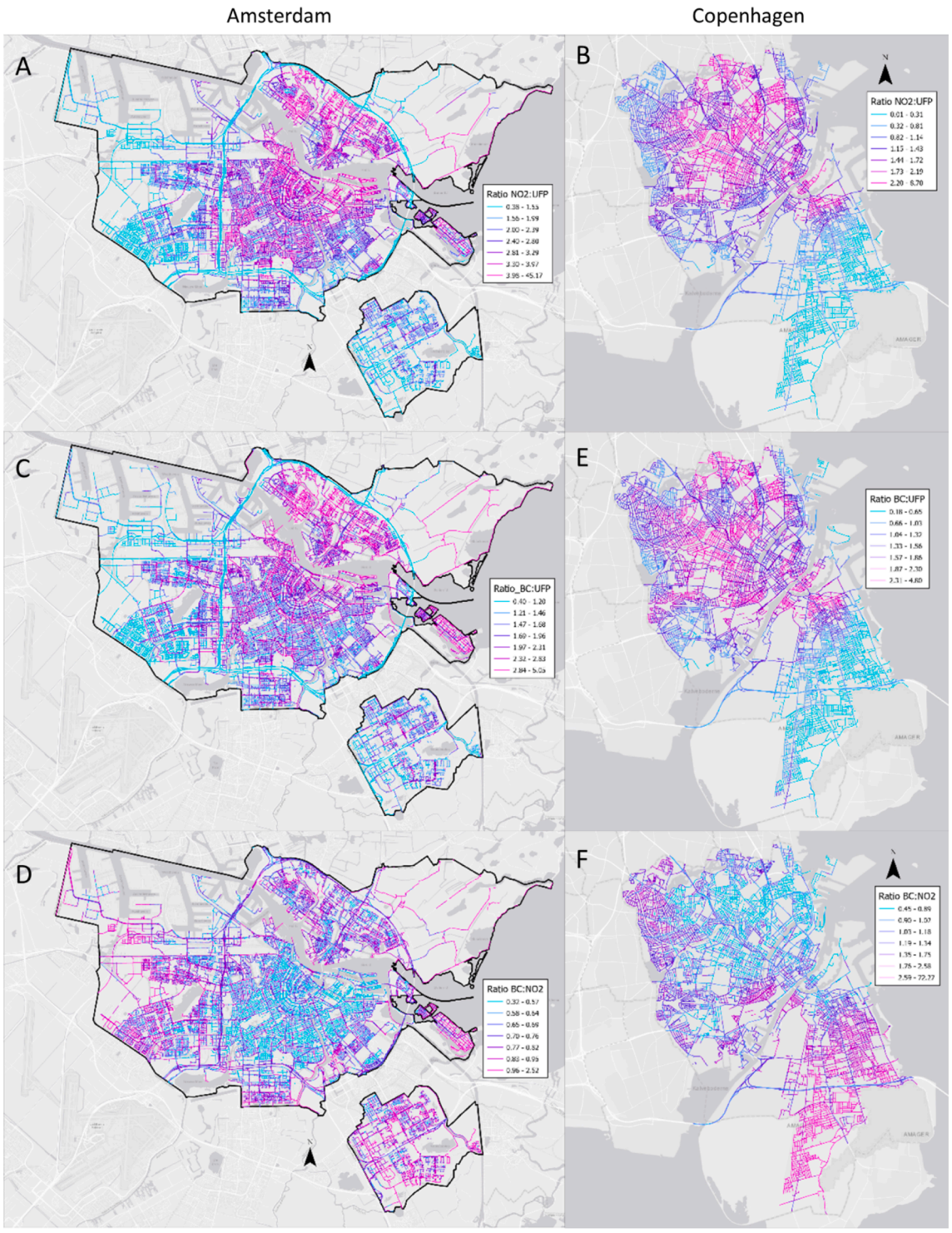

Fig. 5. The ratio between mixed-effect model estimates of two pollutants, that is, (A, B) NO_2 / UFP, (C, D) BC /UFP and (E, F) BC / NO_2 ratios.

3.3.4. *Random-effects*

Fig. S7 shows the random-effect of the mixed-effect model for all pollutants in both cities. Street segments marked red show that the measurements suggested a higher concentration on these streets than a concentration level predicted by the fixed-effect model. Similarly, street segments marked with blue colour suggest lower measured concentrations than the estimated fixed-effect model value. It should be noted that, these observed patterns of the random-effects, however, do not reflect high or low concentrations. Instead, they reflect the locations with fixed-effect model estimates, which can be improved due to a significant difference between the measured data and fixed-effect model estimates. Because of the unbalanced dataset, inherently, mixed-effect model estimates on street segments with more drive days are more likely to deviate from the fixed-effect model as shrinkage in the mixed-effect model depends on the number of measurements and the variance between those measurements. Street segments with a large random-effect also highlight opportunities to reflect on the information that might be missing from the LUR/mixed-effect models, leading to identifications of new sources or updating of emission factors and other input data such as street configuration that could not only improve that

particular street segment but the overall models as well.

One of the examples of uncertainties in the fixed-effect estimates is the ring road in Amsterdam in the southwest of the city. The road has red parts in the south horizontally and blue parts vertically (Fig. S7). The fixed-effect model predicts similar concentration levels for these road sections (around 42,000 particles/cm^3), whereas the measured concentration levels differ (38,000 and 49,000 particles cm^3). This could potentially be due to wrong or missing fixed-effect model inputs or changes in road use at the specific time of the measurements. In this case, the southern horizontal part of the road has recently implemented speed restrictions, resulting in lower UFP concentration levels. Another example is the highway near the airport in Copenhagen (Fig. S7). Here, the measurements suggest higher concentration levels than the fixed-effect UFP predictions, whereas this is much less (or not) the case for NO_2 and BC predictions. Also, the Vesterbro area (Fig. 1) appears to have higher concentrations of BC than the fixed-effect model estimates.

3.3.5. Road classifications

Table 2 shows the differences in NO_2, BC and UFP mixed-effect model estimated concentrations across road types in Amsterdam and Copenhagen. It is clear from Table 2 and Figs. 4 and S4 that the mixed-effect model predictions for all pollutants are higher on highways (motorways) and major (primary) roads. In particular, UFP has significantly elevated values along the highways, which are twice as high as roads classified as primary roads (Table 2). This is due to the increased traffic volume on highways compared to the other roads.

For NO_2 and BC, the difference between highways and major roads is much smaller (i.e., 50 % difference). It is also interesting that concentrations of all pollutants are similar between cities over different road types, except for the residential roads and NO_2 concentrations on motorways. The most significant difference in absolute concentration levels between cities seems to come from the fact that Copenhagen has much more residential roads, resulting in much lower overall concentrations in the city than in Amsterdam (Table 1).

3.4. Strengths and limitations

Due to street-by-street measurements of variation in air pollution, pollution maps can be helpful for both policymakers and epidemiological research. For example, the air pollution maps were previously used in a specific area (Vesterbro; Fig. 1) in Copenhagen to support urban planning (GEHL 2021). In this project, people were discouraged from walking along polluted streets and invited to walk streets with less pollution. Furthermore, Alexeeff et al. (2018) used the high-resolution maps created by GSV cars in Oakland in an epidemiological study. They found that the street-level differences in the long-term exposure to air pollution were associated with a higher risk of cardiovascular events among the elderly.

Using the mixed-effect model to map air pollution is a very scalable approach. This is because the fixed-effect part of the model can be used as a base map, which can be extrapolated to locations without measurements (limited to the geographical domain covered by the measurements). By adding measurements to this map with a mixed-effect model, the base map can update itself on locations where these measurements are robust enough, resulting in random-effects that can change the fixed-effect model estimates. The more precise the on-road measurements are (i.e., less variation in measurements), the more it influences the output. So, with more and more measurements, more local variation can be added to the map. We note that the benefit of the mixed model is only achieved at locations where measurements have been obtained. In non-measured locations, the fixed part of the model (the LUR model) applies, as in classical LUR models. Hence, the benefits are especially realised in study designs with a large number of monitoring locations relative to the number of locations to which the models are applied. Mobile monitoring in which a larger number or even all streets are measured, presents such a setting.

For UFP, it is the first time that a map has been created with measurements on all street segments. So far, maps of only NO, NO_2 and BC have been created with the GSV platform (Apte et al. 2017; Messier et al. 2018). In the previous work without the GSV platform (Kerckhoffs et al. 2017, 2021), we showed that LUR models based on mobile UFP measurements in a selection of streets could assess the spatial variation within a city moderately good ($R^2 = 0.6$), similar to other UFP LUR models in the literature($R^2 > 0.51$) (Hatzopoulou et al. 2017; Minet, Gehr, and Hatzopoulou 2017; Sabaliauskas et al. 2015; Weichenthal et al. 2015). Thus, with the increasing interest in UFP in epidemiology, developing better exposure maps to facilitate health-related studies is essential.

However, it should be noted that the results in this study reflect daytime and on-road concentrations levels (i.e., one “long-term” estimate for each street). For its use in epidemiology, the translation to building facades and exposure over many years, must be considered. As reported in most mobile monitoring studies, on-road measurements are higher than fixed measurements on the side of the road or at the façade of buildings. In our previous mobile monitoring studies of UFP and BC we showed that predictions made by models based on mobile monitoring are about 20–30 % higher than external home-outdoor stationary measurements (Kerckhoffs et al., 2019; Kerckhoffs et al. 2016). Because of dispersion characteristics described earlier, this value is slightly less for NO_2, as it is better homogeneously dispersed due to photochemical reactions. In our associated study, with the mixed-effect model results for NO_2, we found that the mixed-effect model output was about 15–20 % higher than external measurements and predictions. The same gradient was found by Richmond-Bryant et al. (2017) in study in Las Vegas. They found that NO_2 concentrations declined by 16 % between the middle of the road and 10 m from the road (and 21 % for a 20-meter distance).

4. Conclusions

By using a mixed-effect model framework, we were able to develop hyperlocal NO_2, BC, and UFP maps for Amsterdam and Copenhagen based on mobile monitoring. In this mixed-effect model framework, all individual street-level measurements are combined with variables from a linear regression model to remove inaccurate observations. This was needed because for establishing a robust “long-term” concentration estimate, about 9 drive days were needed for NO_2, yielding a relative error of less than 10 percent. For BC and UFP, about 12 drive days were

Table 2
NO_2, UFP and BC mixed-effect model concentrations across road types in Amsterdam and Copenhagen.

	Amsterdam				Copenhagen			
Type of Road*	N	NO_2	UFP	BC	N	NO_2	UFP	BC
Motorway	*1,930*	*54*	*45,400*	*2.84*	*840*	*41*	*49,800*	*2.43*
Primary	*1,721*	*37*	*24,600*	*1.91*	*679*	*34*	*24,600*	*1.94*
Secondary	*3,170*	*32*	*22,300*	*1.69*	*479*	*24*	*21,000*	*1.53*
Tertiary	*4,131*	*28*	*20,800*	*1.47*	*4,454*	*24*	*17,200*	*1.47*
Residential	*11,904*	*25*	*19,700*	*1.21*	*23,412*	*14*	*11,600*	*0.96*

*Type of road according to OpenStreetMap (OSM). Note: N = number of street segments, NO_2 is in μg/m^3, BC is in μg/m^3, and UFP is in particles/cm^3.

needed.

The mixed-effect model, ratio and hotspot maps provided detailed insights into the spatial variation, related to specific sources of NO_2, BC, and UFP exposure. This eventually helps (i) policymakers by zooming into the areas of interest, mainly exploring hyperlocal pollution to create potentially possible adaptations to urban topography (ii) epidemiologists to better differentiate between the health effects of different pollutants.

Overall, the correlation between mixed-effect model estimates of the three pollutants was high and in the range of r = 0.70–0.94. The mixed-effect model predictions showed clear elevated concentration levels for all pollutants on highways and major roads. This was extra pronounced for UFP due to the faster decline of concentration with distance to the source, compared to BC and NO_2. The ratio maps also showed a bigger difference between UFP and BC/NO_2 than between BC and NO_2. This was mainly due to the elevated UFP concentration levels close to airports.

Funding

The project received funding from the Environmental Defense Fund, Google, EXPOSOME-NL (NWO; project number 024.004.017) and EXPANSE (EU-H2020 Grant No 874627). Jibran Khan's work is supported by the Danish Big Data Centre for Environment and Health (BERTHA), funded by the Novo Nordisk Foundation (NNF) Challenge Programme, grant number NNF170C0027864.

Author Contributions

Jules Kerckhoffs: Coordination of data collection, model development for Amsterdam and Copenhagen. **Jibran Khan:** Coordination of input for model development for Copenhagen. **Jules Kerckhoffs & Jibran Khan:** Contributed to the article, data analysis and protocols, software, visualizations, investigations, presentation of results, original draft writing, review – editing and writing. **Ole Hertel, Matthias Ketzel & Steen Solvang Jensen:** Participated in discussions, reviewed and the original draft. **Fares Al Hasan:** Pre-processing of data and GIS information. **Kees Meliefste:** Technical design of measurement platform and study design. **Roel Vermeulen:** Coordinated and designed the study, developed the statistical modelling approach, participated in discussions, reviewed the original draft. **Gerard Hoek and Zhendong Yuan:** Reviewed the original draft.

Declaration of Competing Interest

The authors declare the following financial interests/personal relationships which may be considered as potential competing interests: Jules Kerckhoffs reports financial support was provided by Environmental Defense Fund. Jules Kerckhoffs reports financial support was provided by EXPOSOME-NL. Jules Kerckhoffs reports financial support was provided by EXPANSE. Jibran Khan reports financial support was provided by Danish Big Data Centre for Environment and Health.

Data availability

Data will be made available on request.

Acknowledgements

The authors gratefully acknowledge the help and coordination (data, discussions) of Karin Tuxen-Bettman and Natalie Smailou, Google Inc., USA, during this work. Help, support, and coordination (discussions) of Rasmus Reeh and Christian Gaare Nielsen (Municipality of Copenhagen), Harry van Bergen, Paul Coops, and Imke van Moorselaar (Municipality of Amsterdam) are also thankfully acknowledged.

Appendix A. Supplementary material

Supplementary data to this article can be found online at https://doi.org/10.1016/j.envint.2022.107575.

References

Alexeeff, S.E., Roy, A., Shan, J., Liu, X.i., Messier, K., Apte, J.S., Portier, C., Sidney, S., Van Den Eeden, S.K., 2018. High-resolution mapping of traffic related air pollution with Google street view cars and incidence of cardiovascular events within neighborhoods in Oakland, CA. Environ. Health 17 (1).

Apte, J.S., Messier, K.P., Gani, S., Brauer, M., Kirchstetter, T.W., Lunden, M.M., Marshall, J.D., Portier, C.J., Vermeulen, R.C.H., Hamburg, S.P., 2017. High-Resolution Air Pollution Mapping with Google Street View Cars: Exploiting Big Data. Environ. Sci. Technol. 51 (12), 6999–7008. https://doi.org/10.1021/acs.est.7b00891.

Bischof, Oliver F., Filimundi, E., Bischof, O.F., Bennett, I.P., 2005. The Measurement of Nucleation Mode Particles Using an Ultrafine Water Based CPC. Measurement of Nucleation Mode Particles Using an Ultrafine Water-Based Condensation Particle Counter.

Brines, M., Dall'Osto, M., Beddows, D.C.S., Harrison, R.M., Gómez-Moreno, F., Núñez, L., Artíñano, B., Costabile, F., Gobbi, G.P., Salimi, F., Morawska, L., Sioutas, C., Querol, X., 2015. Traffic and Nucleation Events as Main Sources of Ultrafine Particles in High-Insolation Developed World Cities. Atmos. Chem. Phys. 15 (10), 5929–5945.

Dall'Osto, M., Querol, X., Alastuey, A., O'Dowd, C., Harrison, R.M., Wenger, J., Gómez-Moreno, F.J., 2013. On the Spatial Distribution and Evolution of Ultrafine Particles in Barcelona. Atmos. Chem. Phys. 13 (2), 741–759.

Ellermann, Thomas, Nordstrøm, Claus, Brandt, Jørgen, Christensen, Jesper, Ketzel, Matthias, Massling, Andreas, Bossi, Rossana, Marie, Lise, Camilla, Frohn, Steen, Geels, Jensen, Solvang, Nielsen, Ole-Kenneth, Winther, Morten, Poulsen, Maria Bech, Nygaard, Jesper, Nøjgaard, Jacob Klenø, 2021. Videnskabelig Rapport Fra DCE-Nationalt Center for Miljø Og Energi.

Gani, S., Chambliss, S.E., Messier, K.P., Lunden, M.M., Apte, J.S., 2021. Spatiotemporal Profiles of Ultrafine Particles Differ from Other Traffic-Related Air Pollutants: Lessons from Long-Term Measurements at Fixed Sites and Mobile Monitoring. Environ. Sci.: Atmos. 1 (7), 558–568. https://doi.org/10.1039/D1EA00058F.

GEHL, 2021. Thrive Zone, Copenhagen, Denmark - Gehl. Retrieved September 10, 2021 (https://gehlpeople.com/projects/air-quality-copenhagen/).

Getis, A., Ord, J.K., 1992. The Analysis of Spatial Association by Use of Distance Statistics. Geograph. Anal. 24 (3), 189–206. https://doi.org/10.1111/J.1538-4632.1992.TB00261.X.

Hagler, G., et al., 2009. Ultrafine Particles near a Major Roadway in Raleigh, North Carolina: Downwind Attenuation and Correlation with Traffic-Related Pollutants. Atmos. Environ. 43 (6), 1229–1234. https://doi.org/10.1016/j.atmosenv.2008.11.024.

Hankey, S., Marshall, J.D., 2015. Land Use Regression Models of On-Road Particulate Air Pollution (Particle Number, Black Carbon, PM2.5, Particle Size) Using Mobile Monitoring. Environ. Sci. Technol. 49 (15), 9194–9202. https://doi.org/10.1021/acs.est.5b01209.

Hasenfratz, D., Saukh, O., Walser, C., Hueglin, C., Fierz, M., Arn, T., Beutel, J., Thiele, L., 2015. Deriving High-Resolution Urban Air Pollution Maps Using Mobile Sensor Nodes. Pervasive Mob. Comput. 16, 268–285.

Hatzopoulou, M., Valois, M.F., Levy, I., Mihele, C., Gang, L.u., Bagg, S., Minet, L., Brook, J., 2017. Robustness of Land-Use Regression Models Developed from Mobile Air Pollutant Measurements. Environ. Sci. Technol. 51 (7), 3938–3947. https://doi.org/10.1021/acs.est.7b00366.

Hoek, G., 2017. Methods for Assessing Long-Term Exposures to Outdoor Air Pollutants. Curr. Environ. Health Reports 4 (4), 450–462.

Hofman, J., Staelens, J., Cordell, R., Stroobants, C., Zikova, N., Hama, S.M.L., Wyche, K.P., Kos, G.P.A., Van Der Zee, S., Smallbone, K.L., Weijers, E.P., Monks, P.S., Roekens, E., 2016. Ultrafine Particles in Four European Urban Environments: Results from a New Continuous Long-Term Monitoring Network. Atmos. Environ. 136, 68–81. https://doi.org/10.1016/j.atmosenv.2016.04.010.

Hudda, N., Gould, T., Hartin, K., Larson, T.V., Fruin, S.A., 2014. Emissions from an International Airport Increase Particle Number Concentrations 4-Fold at 10 Km Downwind. Environ. Sci. Technol. 48 (12), 6628–6635. https://doi.org/10.1021/es5001566.

Jones, R.R., Hoek, G., Fisher, J.A., Hasheminassab, S., Wang, D., Ward, M.H., Sioutas, C., Vermeulen, R., Silverman, D.T., 2020. Land Use Regression Models for Ultrafine Particles, Fine Particles, and Black Carbon in Southern California. Sci. Total Environ. 699, 134234 https://doi.org/10.1016/j.scitotenv.2019.134234.

Kerckhoffs, J., Hoek, G., Vermeulen, R., 2019. A Nationwide Land Use Regression Model for Ultrafine Particles. Environ. Epidemiol. 3, 195. doi: 10.1097/01.ee9.0000607960.60423.0e.

Kerckhoffs, J., Hoek, G., Messier, K.P., Brunekreef, B., Meliefste, K., Klompmaker, J.O., Vermeulen, R., 2016. Comparison of Ultrafine Particles and Black Carbon Concentration Predictions from a Mobile and Short-Term Stationary Land-Use Regression Model. Environ. Sci. Technol. 50 (23), 12894–12902. https://doi.org/10.1021/acs.est.6b03476.

Kerckhoffs, J., Hoek, G., Vlaanderen, J., van Nunen, E., Messier, K., Brunekreef, B., Gulliver, J., Vermeulen, R., 2017. Robustness of Intra Urban Land-Use Regression Models for Ultrafine Particles and Black Carbon Based on Mobile Monitoring. Environ. Res. 159, 500–508. https://doi.org/10.1016/j.envres.2017.08.040.

Kerckhoffs, J., Hoek, G., Gehring, U., Vermeulen, R., 2021. Modelling Nationwide Spatial Variation of Ultrafine Particles Based on Mobile Monitoring. Environ. Int. 154 (9), 106569 https://doi.org/10.1016/j.envint.2021.106569.

Kerckhoffs, J., Khan, J., Hoek, G., Yuan, Z., Ellermann, T., Hertel, O., Ketzel, M., Jensen, S.S., Meliefste, K., Vermeulen, R., 2022. Mixed-Effects Modeling Framework for Amsterdam and Copenhagen for Outdoor NO 2 Concentrations Using Measurements Sampled with Google Street View Cars. Environ. Sci. Technol. 56 (11), 7174–7184.

Keuken, M.P., Roemer, M.G.M., Zandveld, P., Verbeek, R.P., Velders, G.J.M., 2012. Trends in Primary NO2 and Exhaust PM Emissions from Road Traffic for the Period 2000–2020 and Implications for Air Quality and Health in the Netherlands. Atmos. Environ. 54, 313–339. https://doi.org/10.1016/J.ATMOSENV.2012.02.009.

Larson, T., Henderson, S.B., Brauer, M., 2009. Mobile Monitoring of Particle Light Absorption Coefficient in an Urban Area as a Basis for Land Use Regression. Environ. Sci. Technol. 43 (13), 4672–5468. https://doi.org/10.1021/es803068e.

Li, H.Z., Gu, P., Ye, Q., Zimmerman, N., Robinson, E.S., Subramanian, R., Apte, J.S., Robinson, A.L., Presto, A.A., 2019. Spatially Dense Air Pollutant Sampling: Implications of Spatial Variability on the Representativeness of Stationary Air Pollutant Monitors. Atmos. Environ: X 2, 100012.

Liu, W., Kaufman, S.L., Osmondson, B.L., Sem, G.J., Quant, F.R., Oberreit, D.R., 2006. Water-Based Condensation Particle Counters for Environmental Monitoring of Ultrafine Particles. J. Air Waste Manag. Assoc. 56 (4), 444–455.

Messier, K.P., Chambliss, S.E., Gani, S., Alvarez, R., Brauer, M., Choi, J.J., Hamburg, S.P., Kerckhoffs, J., Lafranchi, B., Lunden, M.M., Marshall, J.D., Portier, C.J., Roy, A., Szpiro, A.A., Vermeulen, R.C.H., Apte, J.S., 2018. Mapping Air Pollution with Google Street View Cars: Efficient Approaches with Mobile Monitoring and Land Use Regression. Environ. Sci. Technol. 52 (21), 12563–12572. https://doi.org/10.1021/acs.est.8b03395.

Minet, L., Gehr, R., Hatzopoulou, M., 2017. Capturing the Sensitivity of Land-Use Regression Models to Short-Term Mobile Monitoring Campaigns Using Air Pollution Micro-Sensors. Environ. Pollut. 230, 280–290. https://doi.org/10.1016/j.envpol.2017.06.071.

Montagne, D.R., Hoek, G., Klompmaker, J.O., Wang, M., Meliefste, K., Brunekreef, B., 2015. Land Use Regression Models for Ultrafine Particles and Black Carbon Based on Short-Term Monitoring Predict Past Spatial Variation. Environ. Sci. Technol. 49 (14), 8712–8720. https://doi.org/10.1021/es505791g.

Ohlwein, S., Kappeler, R., Joss, M.K., Künzli, N., Hoffmann, B., 2019. Health Effects of Ultrafine Particles: A Systematic Literature Review Update of Epidemiological Evidence. Int. J. Public Health 64 (4), 547–559.

OpenStreetMap contributors, 2021. "OpenStreetMap." Retrieved October 21, 2021 (https://planet.openstreetmap.org/).

Richmond-Bryant, J., Chris Owen, R., Graham, S., Snyder, M., McDow, S., Oakes, M., Kimbrough, S., 2017. Estimation of On-Road NO2 Concentrations, NO2/NOX Ratios, and Related Roadway Gradients from near-Road Monitoring Data. Air Qual. Atmos. Health 10 (5), 611–625. https://doi.org/10.1007/s11869-016-0455-7.

RIVM-LML, 2020. "Luchtmeetnet.Nl." Retrieved June 11, 2021 (https://www.luchtmeetnet.nl/).

Sabaliauskas, K., Jeong, C.H., Yao, X., Reali, C., Sun, T., Evans, G.J., 2015. Development of a Land-Use Regression Model for Ultrafine Particles in Toronto, Canada. Atmos. Environ. 110, 84–92. https://doi.org/10.1016/j.atmosenv.2015.02.018.

Shairsingh, K.K., Jeong, C.H., Wang, J.M., Brook, J.R., Evans, G.J., 2019. Urban Land Use Regression Models: Can Temporal Deconvolution of Traffic Pollution Measurements Extend the Urban LUR to Suburban Areas? Atmos. Environ. 196, 143–151. https://doi.org/10.1016/j.atmosenv.2018.10.013.

Spielman, S.R., Hering, S.V., Kuang, C., Wang, J., 2017. Preliminary Investigation of a Water-Based Method for Fast Integrating Mobility Spectrometry. Aerosol Sci. Technol. 51 (10), 1223–1230. https://doi.org/10.1080/02786826.2017.1338338/SUPPL_FILE/UAST_A_1338338_SM5095.ZIP.

Tavallali, P., Gharibi, H., Singhal, M., Schweizer, D., Cisneros, R., 2020. A Multi-Pollutant Model: A Method Suitable for Studying Complex Relationships in Environmental Epidemiology. Air Qual. Atmos. Health 13 (6), 645–657. https://doi.org/10.1007/S11869-020-00829-3/FIGURES/6.

TSI, 2022. Environmental Particle Counter 3783 | TSI." Retrieved June 10, 2022 (https://tsi.com/products/particle-counters-and-detectors/environmental-particle-counters/environmental-particle-counter-3783/#resources).

Weichenthal, S., Van Ryswyk, K., Goldstein, A., Shekarrizfard, M., Hatzopoulou, M., 2015. Characterizing the Spatial Distribution of Ambient Ultrafine Particles in Toronto, Canada: A Land Use Regression Model. Environ. Pollut. 208, 241–328. https://doi.org/10.1016/j.envpol.2015.04.011.

Zhu, Y., et al., 2009. Air pollutant concentrations near three Texas roadways, Part I: Ultrafine particles. Atmos. Environ. 43 (30) https://doi.org/10.1016/j.atmosenv.2009.04.018.